## ARTICLE   OPEN

# Feedbacks and eddy diffusivity in an energy balance model of tropical rainfall shifts

Henry G. Peterson [1]✉ and William R. Boos [1,2]

Radiative feedbacks are known to strongly modify horizontal shifts of the intertropical convergence zone (ITCZ) produced by remote atmospheric energy sources. This study uses a one-dimensional moist energy balance model to understand how radiative feedbacks and the structure of an imposed eddy diffusivity can influence such ITCZ shifts. The Planck feedback is shown to damp ITCZ shifts more strongly for extratropical forcings than for tropical ones, because lower moisture content in cold regions makes the temperature response larger there. The water vapor feedback on ITCZ shifts is shown to be dominated by changes in the cross-equatorial asymmetry of the relative humidity of subtropical dry zones, with additional contributions by the changes in mixing ratio that occur at fixed relative humidity and by the meridional shift of the humid ITCZ. Finally, the ITCZ response is found to be highly sensitive to the meridional structure of the diffusivity; the ITCZ shift increases with the tropical diffusivity, even when the global mean diffusivity is fixed.

## INTRODUCTION

Atmospheric circulations transport both water and energy, coupling the spatial structure of precipitation to the spatial structure of atmospheric energy transport. When the measure of energy is chosen to include the latent heat stored in water vapor, the net input of this moist energy through the top and bottom of the atmosphere can then be related to the position and intensity of time-mean tropical precipitation maxima, without requiring specification of the latent heat release that accompanies precipitation[1]. Such moist energy frameworks have improved understanding of a variety of tropical climate phenomena, including tropical cyclones, monsoons, and the Madden−Julian Oscillation (see reviews by refs [2–4]).

A salient example of the improved understanding resulting from moist energy frameworks is the recognition that the latitude of the intertropical convergence zone (ITCZ) can be influenced by high-latitude anomalies in the atmospheric moist energy source (e.g. refs [5,6]). Specifically, the zonal mean ITCZ shifts toward an anomalous energy source, in the opposite direction of the cross-equatorial, vertically integrated atmospheric energy flux needed to maintain a steady-state energy balance in the presence of such a forcing[7,8]. This ITCZ shift can be quantitatively diagnosed from the anomalous energy sources and fluxes, through either empirical fits[9] or Taylor expansions for the latitude of the energy flux equator (EFE), defined as the zero line of the zonal mean atmospheric meridional energy transport[10,11]. Related quantitative frameworks have also been used to go beyond the zonal mean and provide information on regional precipitation shifts[12–14]. These studies that relate horizontal shifts in tropical precipitation to anomalous energy sources do not require knowledge of the vertical structures of winds and moist energy content, unlike some of the original moist energy-based frameworks[1,15]; they correspondingly provide no information on changes in the amplitude of the precipitation field.

Most frameworks that relate horizontal shifts in precipitation to anomalous sources of atmospheric moist energy are furthermore diagnostic rather than prognostic: they require knowledge of the net energy source anomaly in order to provide information on the precipitation shift. This is because feedbacks act on any imposed energy source, producing changes in radiative fluxes and in surface turbulent fluxes of latent and sensible heat, altering the horizontal atmospheric energy transport needed to balance the imposed forcing (e.g. refs [8,16,17]). These feedbacks can be large. For example, dynamical ocean heat transports are estimated to damp the zonal mean ITCZ shift by a factor of three compared to what would be achieved in the absence of a dynamical ocean[18,19]. Water vapor provides a positive feedback on the ITCZ shift, consistent with the fact that it provides a positive feedback on the global mean temperature response to a global mean radiative forcing[20–22]. Clouds can provide a positive or negative feedback on ITCZ shifts, at least in numerical models with varying representations of cloud properties[23,24], with the sign of the feedback likely depending on whether the opposing longwave or shortwave cloud feedback dominates (see discussion by ref. [20]).

Here we use a diffusive energy balance model to improve the understanding of the influence of radiative feedbacks on ITCZ shifts produced by localized radiative forcings. We are motivated by the fact that the influence of individual feedbacks on ITCZ shifts remains poorly understood, in part because climate feedbacks have been studied most extensively in the context of the global mean temperature response to global mean radiative forcings (e.g. refs [25–27]). This is not to say that radiative feedbacks on ITCZ shifts have been unexplored; global climate models (GCMs) with idealized and realistic boundary conditions have been used to study the influence of cloud, water vapor (WV), Planck (PL), albedo (AL), and lapse rate (LR) feedbacks on the ITCZ response to imposed forcings[8,17,23,24].

One systematic exploration of an individual feedback was performed by Clark et al.[22] (hereafter C18), who used an idealized GCM to assess the influence of the WV feedback on ITCZ shifts produced by radiative forcings of different magnitudes located in either the tropics or extratropics. Unlike prior studies that

[1]Department of Earth and Planetary Science, University of California, Berkeley, Berkeley, CA, USA. [2]Climate and Ecosystem Sciences Division, Lawrence Berkeley National Laboratory, Berkeley, CA, USA. ✉email: henrygrantpeterson@caltech.edu
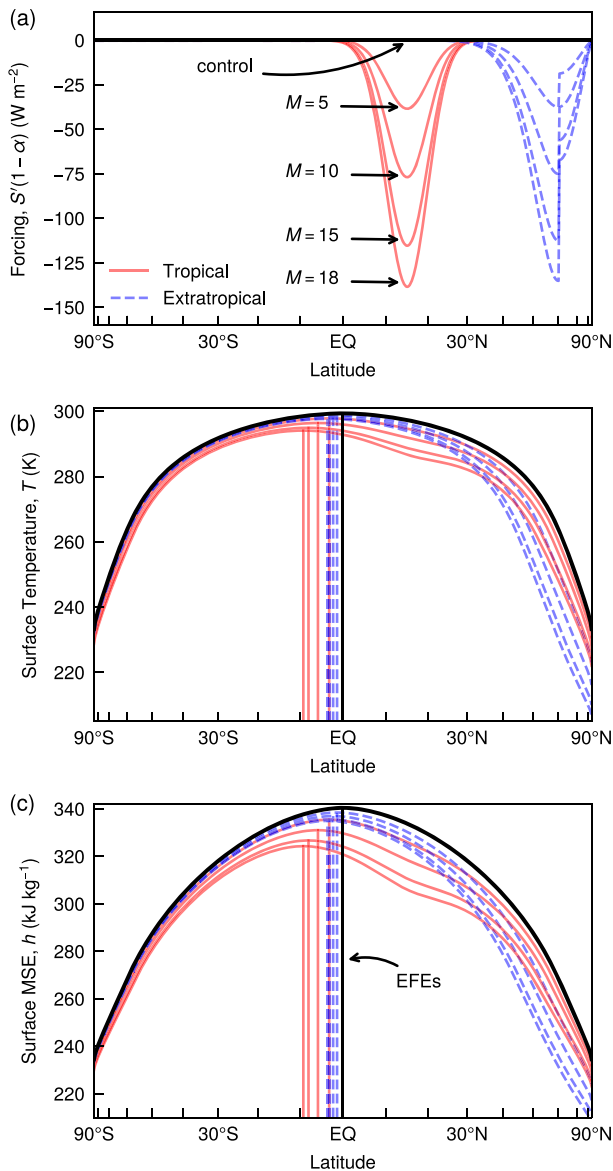
**Fig. 1 The forcings used in sensitivity experiments and examples of the temperature and MSE solutions obtained by the MEBM.** Tropical forcings and responses are in solid red while extratropical are in dashed blue. **a** Forcings, $S'(1 - \alpha)$, for strengths $M = 5$, 10, 15, and 18, including control of $M = S' = 0$. Note that the basic-state albedo alters the effective forcing for the extratropical case. **b** Surface air temperature, $T$, and **c** surface air MSE, $h$, distributions resulting from MEBM simulations with constant diffusivity, $D$, and AL, LR, WV, and PL feedbacks. Vertical lines mark the position of EFEs.

diagnostically estimated the strength of individual feedbacks using a classic climate sensitivity framework (e.g. ref. [28]), C18 used prognostic models (GCMs) with and without the WV feedback to show that this feedback roughly doubled the ITCZ shift produced by a given forcing.

Here we follow a similar methodology, but we use a one-dimensional (1D) moist energy balance model (MEBM) like that employed in studies of the influence of anthropogenic greenhouse gas forcing on poleward energy transports[29], polar amplification of warming[30], and regional climate predictability[31]. Because of the computational efficiency of the MEBM, this allows us to quantify the influence of multiple feedbacks on ITCZ shifts; the diffusive nature of the model also allows us to assess the

comparative importance of diffusive-like transports in different regions. We view this as a small first step toward a theoretical framework that may eventually be used to quantitatively predict feedbacks on ITCZ shifts.

## RESULTS

Here we present results from both an MEBM and a GCM. The MEBM represents the steady-state, vertically integrated moist energy budget in sine-latitude coordinates ($x = \sin\phi$) as

$$-\frac{\partial}{\partial x}\left[D(x)(1 - x^2)\frac{\partial h}{\partial x}\right] = \text{NEI}. \quad (1)$$

The left-hand side represents the vertically integrated divergence of moist energy by the circulation as meridional diffusion of the surface air moist static energy $h$ with diffusivity $D(x)$. The net energy input to each atmospheric column is $\text{NEI} = S(1 - \alpha) - L$, where $S$ is insolation, $\alpha$ is albedo, and $L$ is top-of-atmosphere (TOA) outgoing longwave radiation. The MEBM parameterizes the ice-albedo feedback as a step function of temperature and uses a sophisticated radiative transfer scheme to represent the effects of temperature and water vapor on longwave radiation. The MEBM essentially represents the steady state of a zonal- and annual-mean "aquaplanet", with no land surface or ocean heat transport. We use this MEBM together with a GCM (the Community Earth System Model version 2 (CESM2)) to conduct a series of simulations of the ITCZ shifts produced by remote forcings (see Methods section for more details). We run CESM2 as an entirely oceanic aquaplanet with a 1-m-deep ocean mixed layer. Like the GCM used by C18, our CESM2 model has no sea ice and uses a uniform surface albedo of 0.2725. Neither CESM2 or the MEBM represents cloud-radiative effects, nor did the GCM used by C18.

### Forcings and responses

We apply a series of insolation forcings ($S'$) to both the MEBM and CESM2, taken directly from C18. These are Gaussian energy sinks centered in the northern hemisphere (Fig. 1a). We conduct one set of simulations with perturbations centered at 15°N (labeled "tropical") and another with perturbations centered at 60°N ("extratropical"). Each of these sets contains four simulations with different forcing magnitudes, defined as $-M = \overline{S'}$, with an overbar representing a global mean so that $-M$ represents the prescribed global mean change in insolation. For a given value of $M$, the tropical and extratropical forcings thus produce the same global mean change in insolation. However, for extratropical forcings, the basic-state albedo gradient at the sea ice edge affects the net absorbed shortwave anomaly in the MEBM; our later analyses appropriately normalize for this effect and for the different basic-state albedo in CESM2. Figure 1b, c shows the MEBM's temperature and MSE solutions for each forcing.

To assess the response to these forcings, we find the latitude of the EFE in each simulation. There is no explicit precipitation in the MEBM, and thus no explicit ITCZ, but the latitude of the EFE, $\phi_E$, has been shown to be proportional to the latitude of the ITCZ, $\phi_I$ (e.g. ref. [8]). For the simulations in C18, it was found that $\phi_I = 0.64\phi_E$. For our CESM2 runs, we found that $\phi_I = 0.78\phi_E$ with $r^2 = 0.996$. Because the relation between EFE and ITCZ latitudes seems model-dependent, we analyze EFE shifts and do not explicitly relate these to ITCZ shifts.

### Overview of energy flux equator sensitivities

To quantitatively assess the sensitivity of the EFE to tropical and extratropical forcings, we express each forcing in terms of the cross-equatorial atmospheric energy transport needed to balance the imposed change in insolation in the absence of all feedbacks. Specifically, we follow Kang et al.[8] and meridionally integrate the
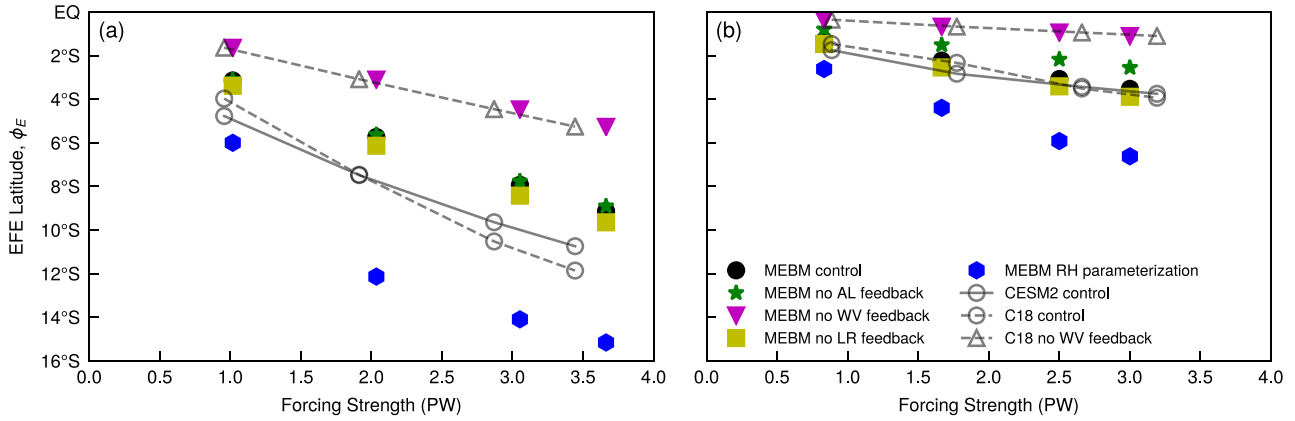
**Fig. 2 EFE shift versus forcing strength for GCM and MEBM simulations. a** Tropical forcings. **b** Extratropical forcings. Forcing strength here is defined as the cross-equatorial transport due to $S'(1 - a)$, or $\mathcal{T}_{S'(1-a)}(0)$ from Eq. (2). Black circles show sensitivity of MEBM with AL, WV, and LR feedbacks active. Other symbols refer to feedback simulations (see Methods section for implementation details). The "RH parameterization" (blue hexagons) is discussed in the section titled "A relative humidity feedback".

forcing after subtracting its global mean value, with the forcing defined as the net absorbed shortwave in the absence of any AL feedback,

$$\mathcal{T}_{S'(1-a)}(x_0) = 2\pi a^2 \int_{-1}^{x_0} \left[ S'(1-a) - \overline{S'(1-a)} \right] dx. \quad (2)$$

Here $a$ is Earth's radius and $x_0$ is the sine of latitude at the basic-state EFE (here equal to zero). The meridional atmospheric energy transport, $\mathcal{T}$ (in PW), is the zonal integral of the meridional vertically integrated atmospheric energy flux, $F$ (in W m$^{-1}$). The forcing, expressed in terms of its cross-equatorial energy transport, is then the equatorial value of $\mathcal{T}_{S'(1-a)}$.

For both tropical and extratropical forcings, the control MEBM has an EFE latitude that exhibits a roughly similar sensitivity to the magnitude of the forcing as both CESM2 and the GCM run by C18 (Fig. 2, compare closed black circles to open gray circles connected by lines). The match between the MEBM and the GCMs is especially close for extratropical forcings, though the sensitivity to those forcings is only about one-third as large as the sensitivity to tropical forcings, consistent with previous model simulations performed without cloud feedbacks (ref. [23], C18). The EFE latitude exhibits some nonlinearity in its relation to forcing amplitude even in the MEBM, but this nonlinearity is greater in the GCMs. For example, CESM2 exhibits a 4.8° EFE shift for a tropical forcing with $M = 5$ W m$^{-2}$, while tripling the magnitude of that forcing only doubles the EFE shift. We discuss reasons for this nonlinearity below, but first we assess linear estimates of these sensitivities and their dependence on feedbacks.

We define the linear response of the EFE to a forcing in terms of the coefficient, $\lambda$, that relates the EFE latitude to the cross-equatorial atmospheric energy transport needed to balance the imposed forcing in the absence of all feedbacks,

$$\lambda = \frac{\phi_E}{\mathcal{T}_{S'(1-a)}}. \quad (3)$$

We calculate $\lambda$ using the smallest forcing ($M = 5$ W m$^{-2}$) to better approximate the linear response. This provides sensitivities between about $-1.5$ and $-5°$ PW$^{-1}$ for the control MEBM and GCMs (see white bars in Fig. 3). Although $\lambda$ has units of ° PW$^{-1}$, it is distinct from the sensitivity estimate of $-3°$ PW$^{-1}$ obtained by Donohoe et al.[9] based on climate models and observations, because Donohoe et al.[9] used the net cross-equatorial energy transport produced by the forcing and all feedbacks, while $\lambda$ references the EFE shift to the forcing alone. This choice of $\lambda$ also accounts for the fact that the albedo is higher in the polar regions of the MEBM's basic state, giving the effective extratropical forcing a smaller global mean value than the tropical forcing (long-dashed
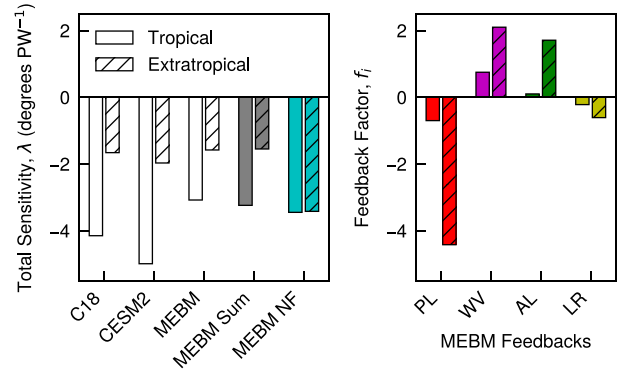


**Fig. 3 Sensitivities for GCMs and the MEBM (left), and feedback factors for the MEBM (right), calculated for tropical (open bars) and extratropical (hatched bars) forcings of magnitude $M = 5$ to reduce nonlinearities.** The sensitivity is defined in Eq. (3) and is shown here for C18, CESM2, and the MEBM (white bars). Feedback factors are described in the Methods section as $f_i = \lambda_{NF} c_i$ where $\lambda_{NF}$ is the linear sensitivity for a system with no feedbacks (shown here under "MEBM NF") and $c_i$ (in units of PW degree$^{-1}$) expresses the linear feedback in terms of a cross-equatorial transport associated with a unit shift in the EFE, holding constant all variables except for $i$ (where $i$ is PL, WV, AL, or LR). The total sensitivity can be approximated as $\lambda \simeq \lambda_{NF}/(1 - \sum_i f_i)$, which is shown here as "MEBM Sum".

lines in Fig. 4); even after accounting for this effect, the sensitivity of the EFE to tropical forcings is still about twice the sensitivity to extratropical forcings (compare open and hatched bars in Fig. 3).

We now estimate the influence of each feedback on the sensitivity of the EFE to the forcings, comparing the response of the EFE in the control MEBM with the response in MEBM simulations in which individual feedbacks were suppressed. Removing the WV feedback strongly decreases the sensitivity of the EFE to both tropical and extratropical forcings, by amounts similar to those seen in the GCM simulations of C18 (Fig. 2, closed purple and open gray triangles). The LR feedback is comparatively weak and, in contrast to the WV feedback, is negative (i.e. increased EFE sensitivity is seen when the LR feedback is suppressed; yellow squares in Fig. 2). The AL feedback (green stars in Fig. 2) has almost no effect on the response to tropical forcings, whereas it provides a positive feedback on extratropical forcings with about half the effect of the WV feedback. In the MEBM, feedbacks on EFE latitude thus have the same sign as they
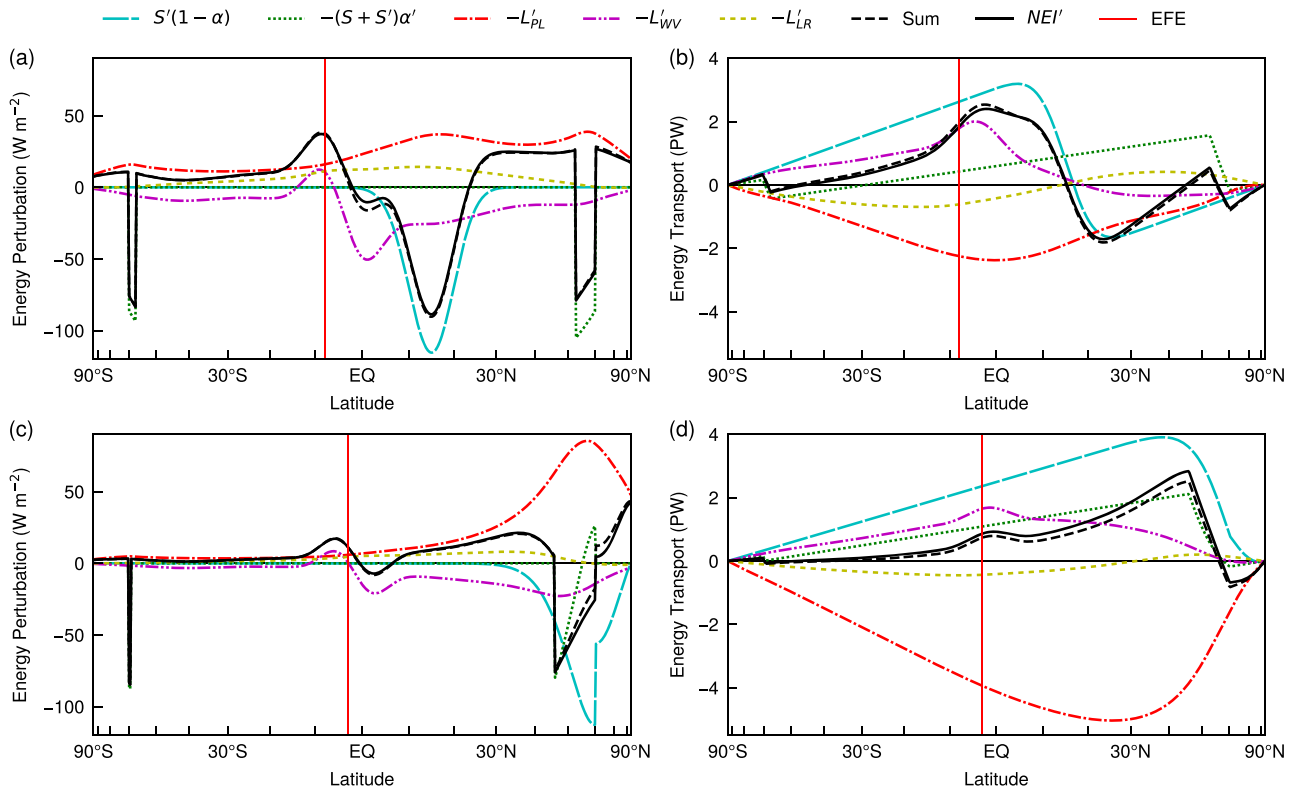
**Fig. 4 Feedback components of longwave and shortwave responses to a forcing and their associated transports.** Panels **a** and **b** show the anomalies and transports, respectively, for a tropical $M = 15$ forcing. The same is shown in **c** and **d** for an extratropical $M = 15$ forcing. "Sum" refers to the sum of the forcing, AL, PL, WV, and LR components and in a linear system would exactly match NEI′. This figure shows results for $M = 15$ forcings to illustrate the nearly linear behavior even for strong forcings.

do when altering the response of global mean surface temperature to a global mean radiative forcing (e.g. ref. [27]).

To present these results more succinctly, one might calculate the contribution of each feedback to the net linear sensitivity parameter as $\lambda_i = (\phi_E - \phi_{E,-i})/\mathcal{T}_{S'(1-\alpha)}$ where $\phi_{E,-i}$ is the EFE from the simulation with feedback $i$ supressed. For instance, for tropical forcings, this gives $\lambda_{WV} = -2.52°$ PW$^{-1}$ for C18 and $\lambda_{WV} = -1.47°$ PW$^{-1}$ for the MEBM. However, these $\lambda_i$ values are analogous to "gains" in a classic feedback analysis framework[32], and gains will not, in general, sum linearly to produce the total $\lambda$. Therefore, we instead follow the climate sensitivity literature and calculate linear feedback factors.

**Quantitative estimates of feedbacks**

We quantify feedback strengths using a basic feedback analysis in which the cross-equatorial energy transport caused by each feedback is assumed to be linearly proportional to the EFE's response,

$$\phi_E = \lambda_{NF}\left(\mathcal{T}_{S'(1-\alpha)} + \sum_i c_i \phi_E\right). \tag{4}$$

Here $\lambda_{NF}$ is the "no-feedback" EFE sensitivity obtained by adding $\mathcal{T}_{S'(1-\alpha)}$ to the energy transport in the full, unforced MEBM, and $c_i$ expresses the linear feedback $i$ in terms of the cross-equatorial energy transport induced by that feedback for a unit shift in the EFE. We estimate $c_i$ as

$$c_i \simeq \frac{\partial \mathcal{T}}{\partial X_i}\frac{dX_i}{d\phi_E}, \tag{5}$$

where the second term on the right-hand side is obtained by finding the total change in parameter $X_i$ (e.g. water vapor, surface

albedo) from a full forced model integration, and the first term on the right is obtained from an offline radiative transfer calculation where all parameters except for $X_i$ are fixed at their values in the full unforced model integration. Each feedback is quantified by a nondimensional feedback factor

$$f_i \equiv \lambda_{NF}c_i. \tag{6}$$

This follows the classic feedback analysis for climate sensitivity reviewed by Roe[32], except that it relates EFE shifts to cross-equatorial energy transport instead of global mean surface temperature to TOA radiation.

We obtain the anomalous energy transport associated with each feedback (i.e. the value of $\mathcal{T}$ in (5)) using the steady-state energy balance,

$$\text{NEI}' = \nabla \cdot F' = \nabla \cdot \left(F_{S'(1-\alpha)} - F_{(S+S')\alpha'} - F_{L'}\right).$$

This expresses the anomalous atmospheric energy flux $F'$ in terms of components whose divergence balances the sum of the forcing, the AL feedback, and all longwave feedbacks (as in the previous section, components of the anomalous transport $\mathcal{T}'$ are obtained by zonally integrating the corresponding component of the anomalous flux $F'$). We furthermore decompose the net change in OLR, $L'$, into components associated with each feedback, which we obtain from the offline radiative transfer calculations mentioned in the previous paragraph. To calculate $L'_{WV}$, for instance, we compute OLR with the perturbed simulation's temperatures but the control simulation's specific humidities, and subtract this from the OLR in the perturbed simulation. The PL feedback is diagnosed by computing OLR for a model state consisting of the forced simulation's water vapor profile and lapse rates, but with surface temperatures matching those of the control simulation. This method of estimating each $c_i$ is a straightforward adaptation of the partial radiative perturbation method used for

estimating the feedbacks that set global mean climate sensitivity[33].

Before we present the feedback factors, we note that summing the $L'_i$ distributions produced by these offline radiative transfer calculations produces a good approximation to the NEI' diagnosed by differencing the perturbed and control models. This confirms that the feedbacks can be diagnosed in this way and linearly superimposed, even for the example of the strong $M = 15\,W\,m^{-2}$ forcing (Fig. 4). That said, there is some nonlinearity in the response to the extratropical forcing due to feedbacks in the northern high-latitudes (cf. solid and dashed black lines in Fig. 4c), and in the response to the tropical forcing due to feedbacks at the equator (Fig. 4a).

The flux form of the feedbacks presented in Fig. 4b, d improves understanding when one recalls that a northward anomalous flux at the location of the basic-state EFE corresponds to an anomalous southward shift of the EFE (e.g. refs [9,10]). For instance, the contribution of the AL feedback to NEI' is very localized compared to that of the WV feedback, but both have similar order-of-magnitude effects on the equatorial $\mathcal{T}'$ for extratropical forcings (Fig. 4d). For tropical forcings, the AL feedback has a small effect on the equatorial $\mathcal{T}'$ and thus a small effect on EFE shifts because its effect on the NEI' has a substantial equatorially symmetric component and also because its northern hemisphere contribution to the NEI' is located further poleward than that for extratropical forcings.

We now present the feedback factors, quantifying the contribution of each radiative feedback to the net EFE sensitivity (Fig. 3). Each $f_i$ has the expected sign, with $f_{WV}$ and $f_{AL}$ being positive while $f_{PL}$ and $f_{LR}$ are negative, but each $f_i$ is much stronger for extratropical than for tropical forcings. The values of $f_{PL}$ and $f_{WV}$ are nearly equal but of opposite sign for tropical forcings, but the amplitude of $f_{PL}$ is about twice that of $f_{WV}$ for extratropical forcings. Using Eqs. (4)–(6), the net EFE sensitivity defined in Eq. (3) can be approximated as

$$\lambda \simeq \frac{\lambda_{NF}}{1 - \sum_i f_i}, \tag{7}$$

as in classic feedback analyses applied to global mean climate sensitivity[32]. This accurately approximates $\lambda$, indicating that the feedbacks behave nearly linearly and supporting the assumptions inherent in Eqs. (4) and (5). For tropical forcings, $\lambda \simeq \lambda_{NF}$, but this seems to be a coincidence due to the approximate cancellation of feedbacks (mostly PL and WV). For extratropical forcings, the smaller EFE sensitivity, with $\lambda$ about half as large as $\lambda_{NF}$, can now be attributed to the much stronger PL feedback on extratropical forcings.

Inspection of the anomalous transport, $\mathcal{T}'$, associated with each feedback provides insight, at least mathematically, on what controls each $f_i$. The equatorial $\mathcal{T}'$ associated with the WV and LR feedbacks is similar for tropical and extratropical forcings (Fig. 4), which combined with the smaller EFE shift for extratropical forcings makes the corresponding values of $c_i$ and $f_i$ larger for extratropical forcings. In contrast, the PL feedback produces a $\mathcal{T}'$ that is about twice as large for extratropical as for tropical forcings. Since $\mathcal{T}'$ is simply the integral of the anomalous TOA radiative flux produced by each feedback, this implies that the hemispherically integrated temperature anomalies are stronger for extratropical than for tropical forcings. We discuss reasons for this in the next subsection.

### Why extratropical forcings cause smaller EFE shifts
The feedback analysis presented above suggests that the smaller EFE shifts produced by extratropical, compared to tropical, forcings occurs because of a stronger PL feedback on extratropical forcings. This is distinct from the argument presented by Seo et al.[23] that, without cloud and water vapor radiative feedbacks,

the diffusive nature of energy transports causes the influence of forcings on EFE latitude to become smaller the further the forcings are from the equator (they also found that a strong cloud feedback can amplify the effects of extratropical forcings to become larger than those of tropical forcings, but neither our models nor that of C18 employ cloud feedbacks). To understand why a larger PL feedback may operate on extratropical forcings, consider the steady, perturbation form of Eq. (1) with NEI' decomposed into forcing and feedbacks,

$$0 = \frac{d}{dy}\left(D\frac{dh'}{dy}\right) + \sum_i b_i T' + S'(1-a), \tag{8}$$

where each $b_i$ is the (potentially spatially varying) feedback parameter for feedbacks linearized in terms of the surface temperature $T'$, and we use Cartesian coordinates in the meridional distance $y$ for simplicity. Roe et al.[31] used the same linearization of feedbacks in a MEBM. We express $h'$ in terms of $T'$ using the Clausius−Clapeyron relation, so that (8) becomes

$$\frac{d}{dy}\left(\kappa\frac{dT'}{dy}\right) + BT' = -S'(1-a), \tag{9}$$

where

$$\kappa = D \cdot \left(c_p + L_v r \frac{\partial q^*}{\partial T}\right) \tag{10}$$

and $B = \Sigma_i b_i$. Here, $c_p$ is the specific heat of air at constant pressure, $L_v$ is the latent heat of vaporization, $r$ is relative humidity, and $q^*$ is the saturation specific humidity. The Clausius−Clapeyron relation provides the value of $\partial_T q^*$, which increases with basic-state temperature at a rate sufficiently rapid to cause $\kappa$ to increase by a factor of 3 between the poles and the equator in our MEBM (not shown).

When expressed in terms of temperature, the perturbation form of our MEBM thus has an apparent diffusivity $\kappa$ that is larger at warmer basic-state temperatures. This is a known feature of EBMs that impose a uniform diffusivity on moist static energy (e.g. ref. [34]) and has been shown to be relevant to the polar amplification of warming that occurs in response to a globally uniform positive radiative forcing (e.g. refs [30,31]). Dynamical atmospheres can also produce a temperature inversion in the polar lower troposphere, resulting in a positive lapse rate feedback that amplifies polar surface temperature anomalies[31,35,36], but this does not occur in our diffusive model which has a prescribed adiabatic lapse rate.

Here we recognize that a smaller temperature diffusivity will result in a $T'$ response that is more spatially confined and of higher amplitude, thus yielding a PL feedback that is more equatorially asymmetric for extratropical forcings. Specifically, Eq. (9) is a simple ODE with Green's function

$$G(y, z) = -\frac{1}{2\kappa\gamma}e^{-\gamma|y-z|},$$

where $\gamma = \sqrt{-B/\kappa}$ is real since $B < 0$. Therefore, the solution to (9) is $T' = G * (-R_f)$ where * is the convolution over all space. For localized forcings such as those used here, this convolution will have maximum magnitude at the center of the forcing and $T'$ will look like a smoothed version of the forcing (we do not plot a full analytical solution here, which would require treatment of the meridional structure in $B$ and $\kappa$, as well as consideration of the spherical domain and polar boundary conditions). The amplitude and meridional width of $T'$ are controlled by the magnitudes of $\kappa$ and $B$; for fixed $B$, increasing $\kappa$ causes $G$ to spread out, reducing the amplitude and increasing the meridional width of $T'$. Since the PL feedback is negative and since all feedbacks produce larger EFE shifts when their contribution to NEI' is more localized on one side of the equator, we expect the PL feedback to have a greater damping
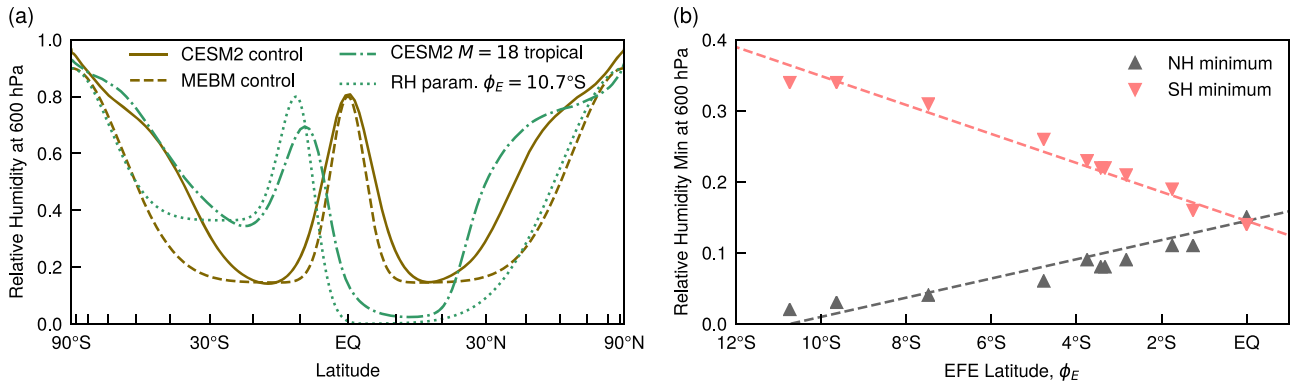
**Fig. 5 Parameterization of an RH feedback from CESM2. a** Latitudinal profile of RH at 600 mb for CESM2 and the MEBM with RH feedback. The CESM2 $M = 18$ tropical forcing simulation (dash-dotted line) has an EFE of $\phi_E = 10.7\,°S$, which we input to our RH feedback parameterization to obtain a profile for the MEBM corresponding to the dotted line. **b** Linear trends of RH minima at 600 mb versus EFE shift for CESM2 simulations. The southern hemisphere (SH) minimum follows a slope of $-0.0204$ with $r^2 = 0.97$, and the northern hemisphere (NH) minimum slope is $0.0145$ with $r^2 = 0.83$. Both fits are forced through the intercept of 0.145 for the control simulation (where $\phi_E = EQ$).

effect on EFE shifts for smaller values of $\kappa$, which in turn are found in colder (i.e. extratropical) parts of the planet. This is consistent with the PL feedback on extratropical forcings having a contribution to NEI′ that is more localized (Fig. 4c) and a flux form with greater magnitude on the equator (Fig. 4d).

This enhanced localization of $T'$ anomalies and the associated larger effect of the PL feedback on EFE shifts occurs in the absence of any rotational confinement of temperature anomalies in our diffusive MEBM. This contrasts with an argument presented by Seo et al.[23], who stated that extratropical forcings produced a larger clear-sky OLR response in their aquaplanet GCM because of a larger Coriolis parameter at higher latitudes: "Since large temperature gradients cannot be sustained in the tropics (e.g. Sobel et al. 2001; Yano and Bonazzola 2009), the tropical thermal forcing … is mostly compensated by atmospheric energy transport divergence with only a small change in TOA radiative fluxes". Furthermore, energy diffusion in the absence of feedbacks cannot explain the smaller sensitivity to extratropical forcings in our MEBM, because the flux form of the forcing, $\mathcal{T}_{S'(1-a)}$, represents the compensating energy transport that would occur in the absence of all feedbacks, and this has nearly the same equatorial value for tropical and extratropical forcings (compare cyan lines in Fig. 4b, d). The total anomalous cross-equatorial transport is smaller for the extratropical forcing (compare black lines in Fig. 4b, d), but this is due to the action of feedbacks, not the purely diffusive, direct response to the forcing (which is represented by the long-dashed cyan lines). Finally, we note that the linearized Planck feedback parameter $b_{PL}$ (which is distinct from the Planck feedback factor, $f_{PL}$, presented in Fig. 3) is expected to be smaller at colder basic-state temperatures, as can be seen by linearizing the Stefan−Boltzmann law: $L' \simeq 4\sigma T^3 T'$. This temperature-dependence of $b_{PL}$ should compensate for some of the decrease in $\kappa$ that occurs in the colder extratropics.

A similar argument applies to the water vapor and lapse rate feedbacks: if these produce a given change in OLR for a unit surface temperature anomaly, the temperature anomaly and thus the OLR change will have a higher local amplitude and be more spatially confined for extratropical forcings than for tropical ones. The meridional diffusivity of temperature is thus expected to set the magnitude of any feedback on EFE latitude that involves a process that alters TOA radiation in response to a local temperature anomaly. This is an important distinction between feedbacks on EFE latitude and feedbacks on surface temperature, and explains why $f_{WV}$ and $f_{LR}$ are also larger for extratropical than for tropical forcings (Fig. 3).

**A relative humidity feedback**

Why is the MEBM less sensitive to tropical forcings than both GCMs, and why does the MEBM respond more linearly to both tropical and extratropical forcings than the GCMs? Examination of the humidity distribution in CESM2 provides a possible answer to these questions: the forcings produce large relative humidity (RH) changes that go beyond a simple meridional shift of the basic-state distribution (compare solid and dash-dotted lines in Fig. 5a). In our default MEBM, the meridional distribution of RH was constructed to change only by shifting meridionally with the EFE, which would naively seem to capture what C18 describe as the main cause of the WV feedback on EFE shifts: "the shift of the water vapor-rich ITCZ into the hemisphere with greater net column heating". However, as the ITCZ shifts southward in CESM2, the low-RH region north of the ITCZ broadens and dries while the low-RH region south of the ITCZ contracts and moistens.

To investigate how important these changes in RH of the dry zones are for the WV feedback, we parameterize them in the MEBM using an empirical fit to CESM2. For all $M$ values, we calculate the best linear fit between the EFE latitude and the 600 hPa zonal mean RH minimum in each hemisphere (Fig. 5b). Then, instead of simply shifting the basic-state RH distribution in the MEBM (that basic-state RH is shown by the dashed line in Fig. 5a), we additionally specify the northern and southern RH minima to vary linearly with EFE latitude. For the example in which $\phi_E = 10.7\,°S$ (corresponding to an $M = 18$ tropical forcing for CESM2), this parameterization produces an equatorial asymmetry in RH in the MEBM that is qualitatively similar to but modestly stronger than that in CESM2 (compare dotted and dash-dotted lines in Fig. 5a). The EFE sensitivity in the MEBM nearly doubles as a result of including this RH parameterization (blue hexagons in Fig. 2), becoming even stronger than that seen in the GCMs (note that these new MEBM simulations also include all other feedbacks). The WV feedback on EFE shifts thus cannot be represented using traditional theory of fixed-RH feedbacks employed for global mean temperature changes, nor can it be thought of as a simple translation of the high-RH region of the ITCZ into the anomalously heated hemisphere.

**Sensitivity to the structure of diffusivity**

We saw above that the meridional structure of the effective temperature diffusivity can alter the strength of temperature-dependent feedbacks on EFE latitude. Might meridional variations in $D$, the moist static energy diffusivity in Eq. (1), be important? Previous studies have shown that if $D$ is diagnosed from idealized GCMs, it is lower in the tropics than in the midlatitudes (e.g.
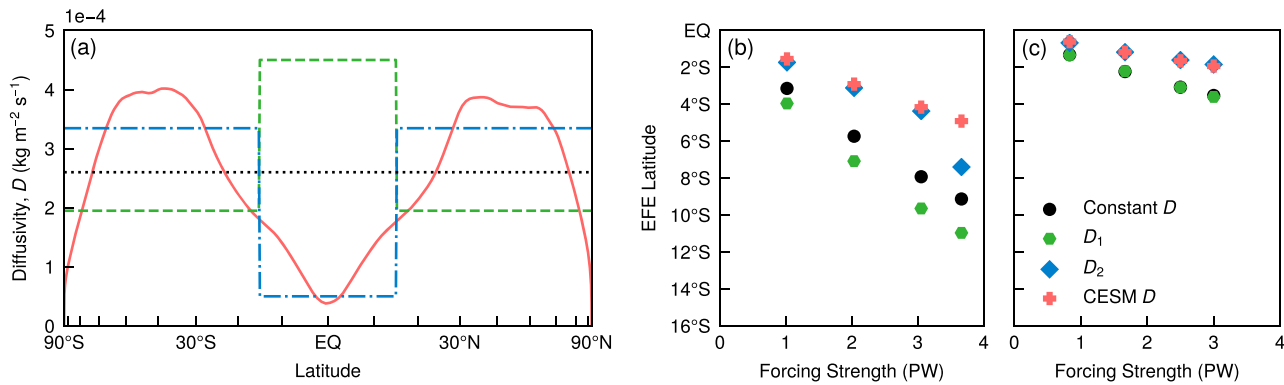
**Fig. 6 MEBM EFE sensitivity for different prescribed temperature diffusivities, $D(x)$. a** Meridional structure of the four diffusivities used. The constant $D$ (dotted) is the same as in Hwang and Frierson[29] and Roe et al.[31], using the units of the latter. Also shown are $D$ diagnosed from CESM2 (solid), $D_1$ (dashed), and $D_2$ (dash-dotted). EFE shifts using these diffusivities are shown in **b** for tropical forcings and **c** extratropical forcings.

ref. [37]). Following those studies, we calculate $D(x)$ for our CESM2 simulations as the coefficient that linearly relates the zonal mean, vertically integrated atmospheric energy flux to the zonal mean $h$; it varies by nearly an order of magnitude, with maxima in the midlatitudes and minima at both the equator and poles (Fig. 6a, solid line). The uniform value of $D$ used in our default MEBM (horizontal dotted line, taken from ref. [29]) approximates the global mean diffusivity in CESM2, but differs from the local $D$ by a factor of five at the equator.

Imposing the distribution of $D(x)$ from CESM2 in our MEBM produces a large weakening of EFE sensitivity to both tropical and extratropical forcings (compare orange crosses to black circles in Fig. 6b, c). For tropical forcings, this reduction in sensitivity is as strong as that obtained by removing the WV feedback.

Motivated by this result, we hypothesize that the diffusivity near the EFE has the largest impact on the EFE sensitivity to a forcing. To test this hypothesis, we perform two additional sets of MEBM simulations with diffusivities $D_1(x)$ and $D_2(x)$, which are square waves with maxima in the tropics and extratropics, respectively, both having the same global mean as the uniform $D$ imposed in our default MEBM (Fig. 6a, dashed and dash-dotted lines). For both tropical and extratropical forcings, simulations using $D_1$ have sensitivities at least as large as those of the constant $D$ simulations, while simulations using $D_2$ have smaller sensitivities (hexagons and diamonds in Fig. 6b, c). The MEBM simulations using $D_2$ have sensitivities nearly the same as the MEBM simulations using the exact $D(x)$ profile diagnosed from CESM2, except for the much larger EFE shift produced for the tropical $M = 18$ forcing; that particular simulation is so cold that sea ice expands to 10°N, causing the AL feedback to dominate. These results suggest that the diffusivity in the tropics has the biggest influence on EFE sensitivity for both tropical and extratropical forcings.

The meridional structure of diffusivity can thus be just as important as climate feedbacks in setting the EFE response to a forcing. A larger near-equatorial diffusivity could produce a larger EFE sensitivity in at least two ways: by increasing the anomaly of cross-equatorial transport induced by a given forcing, or by flattening the basic-state cross-equatorial energy transport and thus increasing the EFE shift that occurs for a given anomaly of cross-equatorial transport (e.g. ref. [10]). The former effect dominates in our MEBM (not shown), seemingly because a larger near-equatorial diffusivity allows $h'$ and gradients in $h'$ (which are proportional to the energy transport) to spread to the equator rather than being confined to off-equatorial regions.

## DISCUSSION
Here we used an MEBM to investigate the influences of climate feedbacks and the eddy diffusivity of moist energy on the sensitivity of the EFE to remote inputs of energy through the top and bottom of the atmosphere. This MEBM has no representation of cloud-radiative effects or the seasonal cycle, which we hope to explore in future work. The MEBM also has no explicit representation of the ITCZ, but the strong correlation between the ITCZ and EFE latitudes in our GCM simulations and those of others (e.g. refs [8,22]) suggests that our MEBM results are highly relevant to ITCZ shifts. The water vapor, lapse rate, Planck, and albedo feedbacks on EFE shifts all have the same sign as they do in the context of the global mean surface temperature response to a global mean radiative forcing, but the magnitude of these feedbacks on EFE shifts depends on whether the forcing is localized in the tropics or extratropics. The albedo feedback is positive and local: it is of moderate strength for extratropical forcings but is negligible for tropical forcings. The lapse rate feedback is negative and is the weakest of all the feedbacks examined here, except for the albedo feedback on tropical forcings.

Two of our most novel results concern the Planck and water vapor feedbacks. As shown in previous work (e.g. refs [30,34]), for a uniform moist energy diffusivity, the effective temperature diffusivity is smaller in colder parts of the planet. This makes the local temperature response, and thus the Planck feedback, larger and more spatially confined for extratropical forcings than for tropical ones. The same reasoning applies to any temperature-dependent feedback (e.g. water vapor and lapse rate), because a smaller temperature diffusivity will cause their influence on TOA radiation to be more confined to one side of the EFE. In our cloud-free MEBM, the greater magnitude of the Planck feedback for extratropical forcings is the primary reason why the EFE shift is smaller for those forcings.

The Planck feedback is opposed by the water vapor feedback, which in the context of the global mean climate sensitivity is known to result from the change in water vapor mixing ratio that occurs at fixed relative humidity (e.g. ref. [38]). Here we find, through comparison of the MEBM with a GCM, that the water vapor feedback on EFE shifts is instead dominated by an increase in the cross-equatorial asymmetry of the relative humidity of the subtropical dry zones, with additional contributions by the changes in water vapor that occur at fixed relative humidity and as the high-relative humidity EFE shifts meridionally.

Finally, we showed that EFE shifts are highly sensitive to the meridional structure of the diffusivity used for moist energy. The EFE shift increases with the magnitude of the tropical diffusivity, even when the global mean diffusivity is fixed. Given that the moist energy diffusivity of GCMs is known to be state-dependent (e.g.

ref. [39]), it seems plausible that diffusivity changes will influence EFE shifts. The diffusivity that acts on anomalies induced by a forcing may even be different from the diffusivity that sets the basic state.

The results from our MEBM show that a given sensitivity of the EFE to remote forcings in a model can result from large, compensating biases in the diffusivity and feedbacks in that model. Our default MEBM may have such compensating biases due to its use of a uniform diffusivity and a weak WV feedback that does not modify the RH of the subtropical dry zones; a more faithful match to the GCMs might be obtained using a diffusivity that is small in the tropics and high in midlatitudes (e.g. $D_2$) together with a strong RH feedback. Similar reasoning might apply when comparing idealized GCMs with the observed atmosphere if, for example, the effective diffusivity is dominated by transient eddies in the former but by stationary eddies in the latter (e.g. ref. [22]). Our results thus show that quantitatively understanding radiative feedbacks may make it possible to truly predict, rather than merely diagnose, the EFE response to a forcing, but that such an effort may also require knowledge of the effective diffusivity that acts on anomalies of both moist energy and temperature.

## METHODS

### Energy balance model

The MEBM, as given in Eq. (1), is represented using a second-order finite difference scheme solved with the multigrid method. As in previous studies[29,31,34,40], this equation represents the balance of the moist energy of a single, bulk atmospheric layer without an explicit ocean or land surface. For simulations with uniform diffusivity, we use $D = 2.6 \times 10^{-4}\,\mathrm{kg\,m^{-2}\,s^{-1}}$. We use a hierarchy of six grids with uniform grid spacings at $\Delta x = 1/512$, 1/256, 1/128, 1/64, 1/32, and 1/16, using injection to go from finer to coarser grids and bilinear interpolation to go from courser to finer grids. The model iterates through $V$-cycles until changes in $h$ are sufficiently small.

The function NEI can be arbitrarily complex in our MEBM, and most of our simulations use a sophisticated longwave radiative transfer scheme while neglecting atmospheric shortwave absorption. This allows for study of a simple ice-albedo feedback and several longwave radiative feedbacks. We omit the radiative effects of clouds, in part because the cloud-radiative feedback is one of the better studied feedbacks on ITCZ shifts (e.g. refs [8,24,41]). In particular, we use

$$S(x) = \frac{S_0}{\pi}\sqrt{1-x^2}, \tag{11}$$

where $S_0 = 1365\,\mathrm{W\,m^{-2}}$, as a simplified insolation, following C18. There are no diurnal or seasonal cycles in the MEBM. The effect of surface ice cover (e.g. ocean sea ice) on albedo is parameterized by

$$a(x) = \begin{cases} 0.2, & T(x) < -10\,^\circ\mathrm{C} \\ 0.6, & T(x) > -10\,^\circ\mathrm{C} \end{cases}, \tag{12}$$

as in North[42]. We repeated many of our simulations using a more complicated shortwave radiative transfer scheme similar to that described below for longwave, but like C18, we did not see appreciable differences in the EFE shifts. We thus opted for the simpler treatment of shortwave, described above, for simplicity.

To represent $L$, we use the Rapid Radiative Transfer Model for GCMs (RRTMG) provided in the climt (Climate Modelling and Diagnostics Toolkit) software package[43], which parameterizes longwave fluxes based on the vertical profiles of temperature and humidity in noninteracting columns with 30 vertical levels. The temperature profile for these columns is taken to be a moist adiabat from surface air temperature $T$, which in turn is obtained from $h$ by assuming a surface air relative humidity (RH) of 0.8.

Above the surface, the RH is prescribed to have idealized vertical and meridional structures drawn from that of GCM aquaplanet simulations (C18 and CESM2, described below). These structures are constructed by first segmenting the atmosphere into a boundary layer (surface to 875 hPa), free troposphere (875 to 200 hPa), tropopause layer (200 hPa and to 100 hPa), and stratosphere (100 hPa and above). In the boundary layer and stratosphere, RH is uniformly set to 0.9 and 0.0, respectively. In the free troposphere and tropopause layers, a meridional structure is set by prescribing RH in terms of Gaussians in $x$. For the free troposphere, we use four Gaussians in $x$ which move together with latitude of the EFE, $\phi_E$, allowing for a moist ITCZ-like column at $\phi_E$ surrounded by dry subtropical

zone s and humid poles. Specifically, a half-Gaussian in RH is prescribed in each of these subdomains: $(-90^\circ, -15^\circ + \phi_E)$, $(-15^\circ + \phi_E, \phi_E)$, $(\phi_E, 15^\circ + \phi_E)$, and $(15^\circ + \phi_E, 90^\circ)$ with the convention that negative latitudes lie south of the equator. We make the spread of each Gaussian small enough so that the magnitude and derivative of RH are approximately the same at the boundaries of the subdomains. At 600 hPa, this yields the dashed line in Fig. 5a. The RH in the tropopause layer is prescribed to be a single Gaussian centered at $\phi_E$ with a spread of 20° latitude, yielding a humid tropics and dry extratropics.

With these choices, the control MEBM has a basic state with surface air temperature varying from 240 K at the poles to 300 K at the equator (Fig. 1b, black line).

### Suppressed-feedback simulations in the MEBM

In additional sets of simulations, we remove individual feedbacks from the forced runs by prescribing the albedo, specific humidity, or lapse rate from the control simulation. For instance, simulations without the AL feedback simply use $a$ from the equilibrated control simulation. The LR feedback is suppressed by prescribing the vertical lapse rate from the equilibrated control simulation, at each latitude, instead of the moist adiabatic lapse rate corresponding to the temperature achieved in the forced simulation. We suppress the WV feedback by using saturation specific humidity, $q^*$, and relative humidity distribution from the control simulation. No prognostic simulations are conducted with a suppressed PL feedback because the model would then be unstable due to the total feedback being positive; the PL feedback is only diagnosed using the offline radiative transfer calculations described in the text.

### General circulation model

We repeated the basic-state simulation and the series of forced simulations (described above), with all longwave feedbacks active, using the atmospheric component of the Community Earth System Model version 2.1.0 (CESM2), a three-dimensional GCM with sophisticated parameterizations of moist convection, radiation, turbulence, and other subgrid-scale processes[44,45]. Specifically, we use the aquaplanet version of the model from the "Simpler Models" initiative[46], with a slab ocean mixed layer and the $1^\circ \times 1^\circ$ finite-volume dynamical core of the Community Atmosphere Model version 6 (CAM6). We employ a 1-m deep ocean mixed layer. These simulations are meant to replicate some of the results of C18, but in a different GCM and one that allows us access to detailed model output; we thus follow C18 and eliminate all cloud-radiative interactions but prescribe a globally uniform surface albedo of 0.2725. There is no sea ice and thus no ice-albedo feedback, so the lower ice-free albedo specified in the MEBM (12) allows the two models to achieve a similar global mean temperature. We impose the same insolation as in the MEBM, although the GCM has an equinoctal diurnal cycle with the instantaneous insolation prescribed to give the time-mean distribution specified in (11).

## REFERENCES

1. Neelin, J. D. & Held, I. M. Modeling tropical convergence based on the moist static energy budget. *Mon. Wea. Rev.* **115**, 3–12 (1987).
2. Neelin, J D. In *Global Circirculation of the Atmosphere*, ed. Schneider, T. and Sobel, A., 267–301 (Princeton University Press, Princeton, NJ, 2007).
3. Zhang, C. Madden−Julian oscillation. *Rev. Geophys.* **43**, RG2003 (2005).
4. Emanuel, K. Tropical cyclones. *Annu. Rev. Earth Planet. Sci.* **31**, 75–104 (2003).
5. Chiang, J. C. H. & Bitz, C. M. Influence of high latitude ice cover on the marine intertropical convergence zone. *Clim. Dyn.* **25**, 477–496 (2005).
6. Broccoli, A. J., Dahl, K. A. & Stouffer, R. J. Response of the ITCZ to Northern Hemisphere cooling. *Geophys. Res. Lett.* **33**, L01702 (2006).

7. Philander, S. G. H. et al. Why the ITCZ is mostly north of the equator. *J. Clim.* **9**, 2958–2972 (1996).

8. Kang, S. M., Held, I. M., Frierson, D. M. W. & Zhao, M. The response of the ITCZ to extratropical thermal forcing: idealized slab-ocean experiments with a GCM. *J. Clim.* **21**, 3521–3532 (2008).

9. Donohoe, A., Marshall, J., Ferreira, D. & Mcgee, D. The relationship between ITCZ location and cross-equatorial atmospheric heat transport: from the seasonal cycle to the last glacial maximum. *J. Clim.* **26**, 3597–3618 (2013).

10. Bischoff, T. & Schneider, T. Energetic constraints on the position of the inter-tropical convergence zone. *J. Clim.* **27**, 4937–4951 (2014).

11. Adam, O., Bischoff, T. & Schneider, T. Seasonal and interannual variations of the energy flux equator and ITCZ. Part I: Zonally averaged ITCZ position. *J. Clim.* **29**, 3219–3230 (2016).

12. Adam, O., Bischoff, T. & Schneider, T. Seasonal and interannual variations of the energy flux equator and ITCZ. Part II: Zonally varying shifts of the ITCZ. *J. Clim.* **29**, 7281–7293 (2016).

13. Boos, W. R. & Korty, R. L. Regional energy budget control of the intertropical convergence zone and application to mid-Holocene rainfall. *Nat. Geosci.* **9**, 892–897 (2016).

14. Lintner, B. R. & Boos, W. R. Using atmospheric energy transport to quantitatively constrain South Pacific convergence zone shifts during ENSO. *J. Clim.* **32**, 1839–1855 (2019).

15. Raymond, D. J. & Fuchs, Ž. Moisture modes and the Madden-Julian oscillation. *J. Clim.* **22**, 3031–3046 (2009).

16. Yoshimori, M. & Broccoli, A. J. Equilibrium response of an atmosphere-mixed layer ocean model to different radiative forcing agents: global and zonal mean response. *J. Clim.* **21**, 4399–4423 (2008).

17. Kang, S. M., Frierson, D. M. W. & Held, I. M. The tropical response to extratropical thermal forcing in an idealized GCM: the importance of radiative feedbacks and convective parameterization. *J. Atmos. Sci.* **6**, 2812–2827 (2009).

18. Schneider, T. Feedback of atmosphere-ocean coupling on shifts of the inter-tropical convergence zone. *Geophys. Res. Lett.* **44**, 11644–11653 (2017).

19. Green, B. & Marshall, J. Coupling of trade winds with ocean circulation damps itcz shifts. *J. Clim.* **30**, 4395–4411 (2017).

20. Yoshimori, M., Yokohata, T. & Abe-Ouchi, A. A comparison of climate feedback strength between CO2 doubling and LGM experiments. *J. Clim.* **22**, 3374–3395 (2009).

21. Cvijanovic, I. & Chiang, J. C. H. Global energy budget changes to high latitude North Atlantic cooling and the tropical ITCZ response. *Clim. Dyn.* **40**, 1435–1452 (2013).

22. Clark, S. K., Ming, Y., Held, I. M. & Phillipps, P. J. The role of the water vapor feedback in the ITCZ response to hemispherically asymmetric forcings. *J. Clim.* **31**, 3659–3678 (2018).

23. Seo, J., Kang, S. M. & Frierson, D. M. W. Sensitivity of intertropical convergence zone movement to the latitudinal position of thermal forcing. *J. Clim.* **27**, 3035–3042 (2014).

24. Voigt, A., Bony, S., Dufresne, J. L. & Stevens, B. The radiative impact of clouds on the shift of the Intertropical Convergence Zone. *Geophys. Res. Lett.* **41**, 4308–4315 (2014).

25. Ramanathan, V. & Coakley, J. A. Climate modeling through radiative-convective models. *Rev. Geophys. Space Phys.* **16**, 465–489 (1978).

26. Charney, J. G. et al. *Carbon Dioxide and Climate* (National Academies Press, Washington, D.C., 1979).

27. Soden, B. & Held, I. An assessment of climate feedbacks in coupled ocean–atmosphere models. *J. Clim.* **19**, 3354–3360 (2006).

28. Yoshimori, M. & Broccoli, A. J. On the link between Hadley circulation changes and radiative feedback processes. *Geophys. Res. Lett.* **36**, 0–4 (2009).

29. Hwang, Y. T. & Frierson, D. M. W. Increasing atmospheric poleward energy transport with global warming. *Geophys. Res. Lett.* **37**, 1–5 (2010).

30. Merlis, T. M. & Henry, M. Simple estimates of polar amplification in moist diffusive energy balance models. *J. Clim.* **31**, 5811–5824 (2018).

31. Roe, G. H., Feldl, N., Armour, K. C., Hwang, Y. T. & Frierson, D. M. W. The remote impacts of climate feedbacks on regional climate predictability. *Nat. Geosci.* **8**, 135–139 (2015).

32. Roe, G. H. Feedbacks, timescales, and seeing red. *Annu. Rev. Earth Planet. Sci.* **37**, 93–115 (2009).

33. Wetherald, R. T. & Manabe, S. Cloud feedback processes in a general circulation model. *J. Atmos. Sci.* **45**, 1397–1415 (2016).

34. Rose, B. E. J., Armour, K. C., Battisti, D. S., Feldl, N. & Koll, D. D. B. The dependence of transient climate sensitivity and radiative feedbacks on the spatial pattern of ocean heat uptake. *Geophys. Res. Lett.* **41**, 1071–1078 (2014).

35. Pithan, F. & Mauritsen, T. Arctic amplification dominated by temperature feedbacks in contemporary climate models. *Nat. Geosci.* **7**, 181–184 (2014).

36. Stuecker, M. F. et al. Polar amplification dominated by local forcing and feedbacks. *Nat. Clim.Change* **8**, 1076–1081 (2018).

37. Frierson, D. M. W., Held, I. M. & Zurita-Gotor, P. A gray-radiation aquaplanet moist GCM. Part II: energy transports in altered climates. *J. Atmos. Sci.* **64**, 1680–1693 (2007).

38. Pierrehumbert, R. T., Brogniez, H. & Roca, R. In *Global Circirculation of the Atmosphere*, ed. Schneider, T. and Sobel, A., 143–185 (Princeton University Press, Princeton, NJ, 2007).

39. Shaw, T. A. & Voigt, A. What can moist thermodynamics tell us about circulation shifts in response to uniform warming? *Geophys. Res. Lett.* **43**, 4566–4575 (2016).

40. Siler, N., Roe, G. H. & Armour, K. C. Insights into the zonal-mean response of the hydrologic cycle to global warming from a diffusive energy balance model. *J. Clim.* **31**, 7481–7493 (2018).

41. Voigt, A., Stevens, B., Bader, J. & Mauritsen, T. Compensation of hemispheric albedo asymmetries by shifts of the ITCZ and tropical clouds. *J. Clim.* **27**, 1029–1045 (2014).

42. North, G. R. Theory of energy-balance models. *J. Atmos. Sci.* **32**, 2033–2043 (1975).

43. Monteiro, J. M., Mcgibbon, J. & Caballero, R. sympl (v. 0.4.0) and climt (v. 0.15.3)—towards a flexible framework for building model hierarchies in Python. *Geosci. Model Dev.* **11**, 3781–3794 (2018).

44. Neale, R. B. et al. Description of the NCAR Community Atmosphere Model (CAM 5.0). Ncar/Tn-464+Str (2012).

45. Hurrell, J. W. et al. The community earth system model: a framework for collaborative research. *Bull. Am. Meteorol. Soc.* **94**, 1339–1360 (2013).

46. Medeiros, B., Williamson, D. L. & Olson, J. G. Reference aquaplanet climate in the Community Atmosphere Model, Version 5. *J. Adv. Model. Earth Syst.* **8**, 406–424 (2016).

## ACKNOWLEDGEMENTS

## AUTHOR CONTRIBUTIONS

W.R.B. conceived the project, but both authors designed the study, the modelling strategy, and the analyses. H.G.P. developed the MEBM. W.R.B. ran CESM2. Both authors wrote the manuscript.

## COMPETING INTERESTS

The authors declare no competing interests.

## ADDITIONAL INFORMATION

**Correspondence** and requests for materials should be addressed to H.G.P.

**Reprints and permission information** is available at http://www.nature.com/reprints

**Publisher's note** Springer Nature remains neutral with regard to jurisdictional claims in published maps and institutional affiliations.